An Efficient and Accurate Numerical Method of Stress Intensity Factors Calculation of a Branched Crack

Xiangqiao Yan
Research Laboratory on Composite Materials,
Harbin Institute of Technology,
Harbin 150001, P.R. China

Based on the analytical solution of Crouch to the problem of a constant discontinuity in displacement over a finite line segment in an infinite elastic solid, in the present paper, the crack-tip displacement discontinuity elements, which can be classified as the left and the right crack-tip elements, are presented to model the singularity of stress near a crack tip. Furthermore, the crack-tip elements together with the constant displacement discontinuity elements presented by Crouch and Starfied are used to develop a numerical approach for calculating the stress intensity factors (SIFs) of general plane cracks. In the boundary element implementation, the left or the right crack-tip element is placed locally at the corresponding left or right crack tip on top of the constant displacement discontinuity elements that cover the entire crack surface and the other boundaries. The method is called the hybrid displacement discontinuity method (HDDM). Numerical examples are given and compared with the available solutions. It can be found that the numerical approach is simple, yet very accurate for calculating the SIFs of branched cracks. As a new example, cracks emanating from a rhombus hole in an infinite plate under biaxial loads are taken into consideration. The numerical results indicate the efficiency of the present numerical approach and can reveal the effect of the biaxial load on the SIFs. In addition, the hybrid displacement discontinuity method together with the maximum circumferential stress criterion (Erdogan and Sih) becomes a very effective numerical approach for simulating the fatigue crack propagation process in plane elastic bodies under mixed-mode conditions. In the numerical simulation, for each increment of crack extension, remeshing of existing boundaries is not required because of an intrinsic feature of the HDDM. Crack propagation is simulated by adding new boundary elements on the incremental crack extension to the previous crack boundaries. At the same time, the element characters of some related elements are adjusted according to the manner in which the boundary element method is implemented. [DOI: 10.1115/1.1796449]

1 Introduction

Among the different configurations of branched cracks, the singly branched crack, as shown in Fig. 1, has received the most attention in the literature. There have been many attempts [1–12] to solve this problem for arbitrarily values of a/b, the ratio of the half-crack length a of the main crack to the branch crack length b. Of particular physical interest is the limiting case as $a/b \rightarrow \infty$, where the solution [3,4] has been used to predict the initial angle of the branching of a crack in brittle solids under mixed-mode loading.

The majority of the analyses on branched cracks were based on the Muskhelishvili potential formulation and conformal mapping of the branched crack geometry. With the development of numerical computational techniques, numerical methods, in particular, finite element methods and boundary element methods are used extensively in solving the crack problems. It is well known that how to model the crack is the key issue in the analyses. Among several elastic two-dimensional crack modeling strategies by the boundary element methods, there exist the multidomain formulation [13], the stress formulation with regularization [14], and the dual boundary element method [15,16]. For each formulation, in order to model the singularity of stress near a crack tip, options are available such as building in the crack-tip stress singularity [17], using the quarter-point boundary element [13], and strategically refining the near-crack-tip nonsingular element. Further details on elastic crack analysis by the boundary element method are given in Refs. [18], [19].

Even though much achievement has been made in crack-modeling techniques, both simple and very accurate crack-modeling techniques still need to be developed, in particular for branched crack problems and crack propagation problems. The displacement discontinuity boundary element method [20,21] is very well suited for analyzing plane crack problems because, physically, one can imagine a displacement discontinuity as a line crack whose opposing surfaces are displaced relative to one another. Based on the analytical solution [21] to the problem of a constant discontinuity in displacement over a finite line segment in an infinite elastic solid, in the present paper, the crack-tip displacement discontinuity elements, which can be classified as the left and the right crack-tip displacement discontinuity elements, are presented to model the singularity of stress near a crack tip. Furthermore, the crack-tip elements together with the constant displacement discontinuity elements presented by Crouch and Starfied are used to develop a numerical approach for calculating the stress intensity factors (SIFs) of general plane cracks. In the boundary element implementation, the left or the right crack-tip element is placed locally at the corresponding left or right crack

Contributed by the Applied Mechanics Division of THE AMERICAN SOCIETY OF MECHANICAL ENGINEERS for publication in the ASME JOURNAL OF APPLIED MECHANICS. Manuscript received by the ASME Applied Mechanics Division, September 16, 2002; final revision, May 5, 2004. Associate Editor: H. Gao. Discussion on the paper should be addressed to the Editor, Prof. Robert M. McMeeking, Journal of Applied Mechanics, Department of Mechanical and Environmental Engineering, University of California—Santa Barbara, Santa Barbara, CA 93106-5070, and will be accepted until four months after final publication of the paper itself in the ASME JOURNAL OF APPLIED MECHANICS.

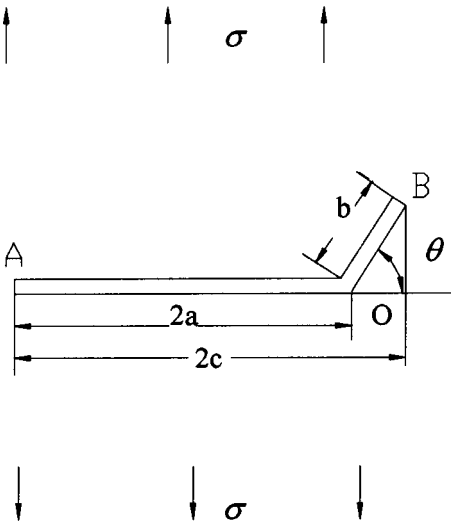

Fig. 1 A singly branched crack

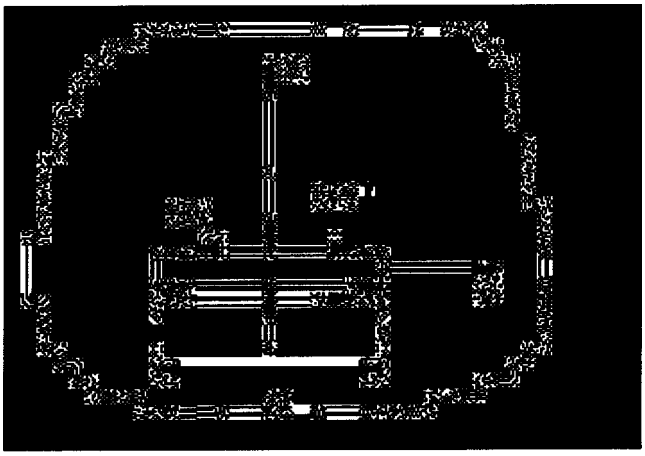

Fig. 2 Schematic of constant displacement discontinuity components D_x and D_y

tip on top of constant displacement discontinuity elements that cover the entire crack surface and the other boundaries. The method is called the hybrid displacement discontinuity method (HDDM). Numerical examples are given and compared with the available solutions. It can be seen that the numerical approach is simple, yet very accurate for calculating the SIFs of branched cracks. As a new example, cracks emanating from a rhombus hole in an infinite plate under biaxial loads are taken into account. The numerical results indicate the efficiency of the present numerical approach and can reveal the effect of the biaxial load on the SIFs.

On the application of boundary element methods to crack propagation analysis, the first attempt to automatically model crack propagation under mixed-mode conditions was given by Ingraffea, Blandford, and Liggett [22] for two-dimensional problems. They used the multiregion method [13] together with the maximum circumferential stress criterion to calculate the direction of crack propagation. Aliabadi [23] pointed out that the difficulty with the multiregion method is that the introduction of artificial boundaries to divide the regions is not unique, and that thus it is not easy to implement it in an automatic procedure. In an incremental crack extension analysis, these artificial boundaries must be repeatedly introduced for each increment of crack extension. In this paper, the hybrid displacement discontinuity method together with the maximum circumferential stress criterion [24] becomes a very effective numerical approach for simulating the fatigue crack propagation process in plane elastic bodies under mixed-mode conditions. In the numerical simulation, for each increment of crack extension, remeshing of existing boundaries is not required because of an intrinsic feature of the HDDM. Crack propagation is simulated by adding new boundary elements on the incremental crack extension to the previous crack boundaries. At the same time, the element characters of some related elements are adjusted according to the manner in which the boundary element method is implemented. As an example, the fatigue propagation process of cracks emanating from a circular hole in a plane elastic plate is simulated using the numerical simulation approach.

By the way, it is pointed out here that finite element simulations [25,26] when used to analyze crack problems have to face large computational problems connected with the discretization of the continuum into finite elements, particularly when some cracks propagate, thus changing the interior boundaries of the solids.

2 The Hybrid Displacement Discontinuity Method

The numerical approach presented in this paper for calculating the SIFs of branched cracks consists of the constant displacement discontinuity elements presented by Crouch and Starfield [20] and the crack-tip displacement discontinuity elements proposed herein.

2.1 Theoretical Foundation of the Constant Displacement Discontinuity Element. The problem of a constant displacement discontinuity over a finite line segment in the (x, y) plane of an infinite elastic solid is specified by the condition that the displacements be continuous everywhere except over the line segment in question. The line segment may be chosen to occupy a certain portion of the x axis, say the portion $|x|<a$, $y=0$. If we consider this segment to be a line crack, we can distinguish its two surfaces by saying that one surface is on the *positive* side of $y=0$, denoted $y=0_+$, and the other is on the *negative* side, denoted $y=0_-$. In crossing from one side of the line segment to the other, the displacements undergo a *constant* specified change in value $D_i=(D_x,D_y)$.

The displacement discontinuities D_i are defined as the difference in displacement between the two sides of the segment:

$$\begin{aligned} D_x&=u_x(x,0_-)-u_x(x,0_+),\\ D_y&=u_y(x,0_-)-u_y(x,0_+). \end{aligned} \tag{1}$$

Because u_x and u_y are positive in the positive x and y coordinate directions, it follows that D_x and D_y are positive as illustrated in Fig. 2. The solution to the subject problem is given by Crouch [21]. The displacements and stresses can be written as

$$\begin{aligned} u_x&=D_x[2(1-\nu)F_3(x,y,a)-yF_5(x,y,a)]\\ &\quad+D_y[-(1-2\nu)F_2(x,y,a)-yF_4(x,y,a)],\\ u_y&=D_x[(1-2\nu)F_2(x,y,a)-yF_4(x,y,a)]\\ &\quad+D_y[2(1-\nu)F_3(x,y,a)-yF_5(x,y,a)], \end{aligned} \tag{2}$$

and

$$\begin{aligned} \sigma_{xx}&=2GD_x[2F_4(x,y,a)+yF_6(x,y,a)]\\ &\quad+2GD_y[-F_5(x,y,a)+yF_7(x,y,a)],\\ \sigma_{yy}&=2GD_x[-yF_6(x,y,a)]\\ &\quad+2GD_y[-F_5(x,y,a)-yF_7(x,y,a)],\\ \sigma_{xy}&=2GD_x[-F_5(x,y,a)\\ &\quad+yF_7(x,y,a)]+2GD_y[-yF_6(x,y,a)]. \end{aligned} \tag{3}$$

Functions F_2 through F_7 in these equations are

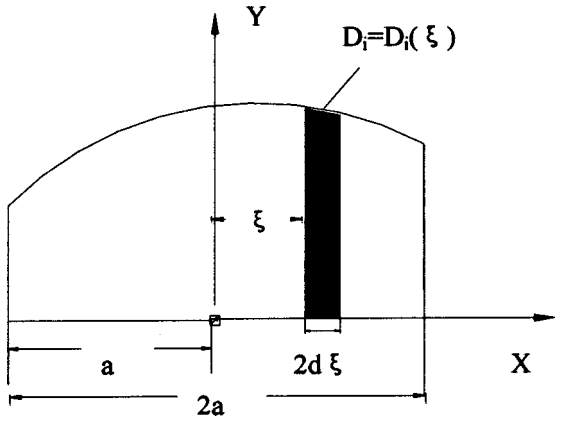

Fig. 3 Schematic of an arbitrary displacement discontinuity function and its differential element

$$
\begin{aligned}
F_2(x,y,a) &= f_{,x} = \frac{1}{4\pi(1-\nu)} \\
&\quad \times [\ln\sqrt{(x-a)^2+y^2} - \ln\sqrt{(x+a)^2+y^2}], \\
F_3(x,y,a) &= f_{,y} = -\frac{1}{4\pi(1-\nu)}\left[\arctan\frac{y}{x-a} - \arctan\frac{y}{x+a}\right], \\
F_4(x,y,a) &= f_{,xy} = \frac{1}{4\pi(1-\nu)}\left[\frac{y}{(x-a)^2+y^2} - \frac{y}{(x+a)^2+y^2}\right], \\
F_5(x,y,a) &= f_{,xx} = -f_{,yy} \\
&= \frac{1}{4\pi(1-\nu)}\left[\frac{x-a}{(x-a)^2+y^2} - \frac{x+a}{(x+a)^2+y^2}\right], \\
F_6(x,y,a) &= f_{,xyy} = -f_{,xxx} \\
&= \frac{1}{4\pi(1-\nu)}\left[\frac{(x-a)^2-y^2}{\{(x-a)^2+y^2\}^2} - \frac{(x+a)^2-y^2}{\{(x+a)^2+y^2\}^2}\right], \\
F_7(x,y,a) &= f_{,yyy} = -f_{,xxy} \\
&= \frac{2y}{4\pi(1-\nu)}\left[\frac{x-a}{\{(x-a)^2+y^2\}^2} - \frac{x+a}{\{(x+a)^2+y^2\}^2}\right],
\end{aligned}
\tag{4}
$$

where

$$
\begin{aligned}
f(x,y) = \frac{-1}{4\pi(1-\nu)}\Bigg[& y\left(\arctan\frac{y}{x-a} - \arctan\frac{y}{x+a}\right) \\
& - (x-a)\ln\sqrt{(x-a)^2+y^2} + x + a\ln\sqrt{(x+a)^2+y^2}\Bigg].
\end{aligned}
\tag{5}
$$

G and ν in these equations are shear modulus and the Poisson's ratio, respectively. Equations (2) and (3) are used by Crouch and Starfield [20] to set up a constant displacement discontinuity boundary element method.

2.2 Basic Formulas Required to Set Up a Higher Displacement Discontinuity Element. Now, consider arbitrary displacement discontinuity distributions along element length $2a$, as shown in Fig. 3:

$$D_i = D_i(\xi) \quad (i=1,2) \tag{6a}$$

or

$$D_x = D_x(\xi), \quad D_y = D_y(\xi). \tag{6b}$$

Based on the solution of the constant discontinuity in displacement given by Crouch [21], the displacements and stresses at a point (x, y) due to a *differential element* with its length $2d\xi$ and its center ξ (see Fig. 3) can be obtained from a differential viewpoint:

$$
\begin{aligned}
du_x &= D_x(\xi)[2(1-\nu)T_3(x,y,\xi,d\xi) - yT_5(x,y,\xi,d\xi)] \\
&\quad + D_y(\xi)[-(1-2\nu)T_2(x,y,\xi,d\xi) - yT_4(x,y,\xi,d\xi)], \\
du_y &= D_x(\xi)[(1-2\nu)T_2(x,y,\xi,d\xi) - yT_4(x,y,\xi,d\xi)] \\
&\quad + D_y(\xi)[2(1-\nu)T_3(x,y,\xi,d\xi) - yT_5(x,y,\xi,d\xi)],
\end{aligned}
\tag{7}
$$

and

$$
\begin{aligned}
d\sigma_{xx} &= 2GD_x(\xi)[2T_4(x,y,\xi,d\xi) + yT_6(x,y,\xi,d\xi)] \\
&\quad + 2GD_y(\xi)[-T_5(x,y,\xi,d\xi) + yT_7(x,y,\xi,d\xi)], \\
d\sigma_{yy} &= 2GD_x(\xi)[-yT_6(x,y,\xi,d\xi)] \\
&\quad + 2GD_y(\xi)[-T_5(x,y,\xi,d\xi) - yT_7(x,y,\xi,d\xi)], \\
d\sigma_{xy} &= 2GD_x(\xi)[-T_5(x,y,\xi,d\xi) \\
&\quad + yT_7(x,y,\xi,d\xi)] + 2GD_y(\xi)[-yT_6(x,y,\xi,d\xi)].
\end{aligned}
\tag{8}
$$

Functions T_2 and T_7 in these equations are given by

$$
\begin{aligned}
T_2(x,y,\xi,d\xi)/d\xi &= V_2(x,y,\xi) = -\frac{1}{4\pi(1-\nu)}\frac{x-\xi}{(x-\xi)^2+y^2}, \\
T_3(x,y,\xi,d\xi)/d\xi &= V_3(x,y,\xi) = -\frac{1}{4\pi(1-\nu)}\frac{y}{(x-\xi)^2+y^2}, \\
T_4(x,y,\xi,d\xi)/d\xi &= V_4(x,y,\xi) = \frac{2y}{4\pi(1-\nu)}\frac{x-\xi}{\{(x-\xi)^2+y^2\}^2}, \\
T_5(x,y,\xi,d\xi)/d\xi &= V_5(x,y,\xi) = \frac{1}{4\pi(1-\nu)}\frac{(x-\xi)^2-y^2}{\{(x-\xi)^2+y^2\}^2}, \\
T_6(x,y,\xi,d\xi)/d\xi &= V_6(x,y,\xi) \\
&= \frac{2}{4\pi(1-\nu)}\left\{\frac{(x-\xi)^3}{[(x-\xi)^2+y^2]^3} - \frac{3(x-\xi)y^2}{[(x-\xi)^2+y^2]^3}\right\}, \\
T_7(x,y,\xi,d\xi)/d\xi &= V_7(x,y,\xi) \\
&= \frac{2y}{4\pi(1-\nu)}\left\{\frac{3(x-\xi)^2}{[(x-\xi)^2+y^2]^3} - \frac{y^2}{[(x-\xi)^2+y^2]^3}\right\}.
\end{aligned}
\tag{9}
$$

Obviously, if the following integrals are obtained,

$$U_{ij}(x,y,a) = \int_{-a}^{a} D_j(\xi)V_i(x,y,\xi)d\xi \quad (i=2,3,\ldots,7;\ \ j=1,2) \tag{10}$$

the displacements and stresses at a point (x, y) due to the whole element can be written as

$$
\begin{aligned}
u_x &= [2(1-\nu)U_{3x}(x,y,a) - yU_{5x}(x,y,a)] \\
&\quad + [-(1-2\nu)U_{2y}(x,y,a) - yU_{4y}(x,y,a)], \\
u_y &= [(1-2\nu)U_{2x}(x,y,a) - yU_{4x}(x,y,a)] \\
&\quad + [2(1-\nu)U_{3y}(x,y,a) - yU_{5y}(x,y,a)],
\end{aligned}
\tag{11}
$$

and

$$
\begin{aligned}
\sigma_{xx} &= 2G[2U_{4x}(x,y,a) + yU_{6x}(x,y,a)] \\
&\quad + 2G[-U_{5y}(x,y,a) + yU_{7y}(x,y,a)],
\end{aligned}
$$

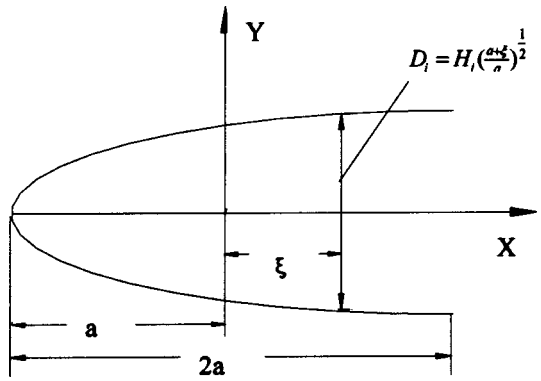

Fig. 4 Schematic of the left crack-tip displacement discontinuity element

$$\begin{aligned}\sigma_{yy}&=2G[-yU_{6x}(x,y,a)]\\&\quad+2G[-U_{5y}(x,y,a)-yU_{7y}(x,y,a)],\\\sigma_{xy}&=2G[-U_{5x}(x,y,a)\\&\quad+yU_{7x}(x,y,a)]+2G[-yU_{6y}(x,y,a)].\end{aligned}\tag{12}$$

The formulas (9)–(12) are the basic formulas required to set up a higher displacement discontinuity element.

2.3 Crack-Tip Displacement Discontinuity Elements. Here, the basic formulas (9)–(12) are used to set up the crack-tip displacement discontinuity elements, which can be classified as the left and the right crack-tip displacement discontinuity elements, to deal with general plane crack problems. The schematic of the left crack-tip displacement discontinuity element is shown in Fig. 4. Its displacement discontinuity functions are chosen as

$$D_x=H_s\left(\frac{a+\xi}{a}\right)^{1/2},\quad D_y=H_n\left(\frac{a+\xi}{a}\right)^{1/2},\tag{13}$$

where H_s and H_n are the tangential and normal displacement discontinuity quantities at the center of the element, respectively. Here, it is noted that the element has the same unknowns as the two-dimensional constant displacement discontinuity element. But it can be seen that the displacement discontinuity functions defined in Eqs. (13) can model the displacement field around the crack tip. The stress field determined by the displacement discontinuity functions (13) possesses $r^{-1/2}$ singularity around the crack tip.

After substituting Eqs. (13) into (10), one has

$$U_{ij}(x,y,a)=H_j\int_{-a}^{a}\left(\frac{a+\xi}{a}\right)^{1/2}V_i(x,y,\xi)d\xi=H_jB_i(x,y,a)\quad(i=2,3,\ldots,7;\ \ j=1,2),\tag{14}$$

where

$$B_i(x,y,a)=\int_{-a}^{a}\left(\frac{a+\xi}{a}\right)^{1/2}V_i(x,y,\xi)d\xi\quad(i=2,3,\ldots,7).\tag{15}$$

After substituting Eq. (14) into Eqs. (11) and (12), one can obtain

$$\begin{aligned}u_x&=H_s[2(1-\nu)B_3(x,y,a)-yB_5(x,y,a)]\\&\quad+H_n[-(1-2\nu)B_2(x,y,a)-yB_4(x,y,a)],\\u_y&=H_s[(1-2\nu)B_2(x,y,a)-yB_4(x,y,a)]\\&\quad+H_n[2(1-\nu)B_3(x,y,a)-yB_5(x,y,a)],\end{aligned}\tag{16}$$

and

$$\begin{aligned}\sigma_{xx}&=2GH_s[2B_4(x,y,a)+yB_6(x,y,a)]\\&\quad+2GH_n[-B_5(x,y,a)+yB_7(x,y,a)],\\\sigma_{yy}&=2GH_s[-yB_6(x,y,a)]\\&\quad+2GH_n[-B_5(x,y,a)-yB_7(x,y,a)],\\\sigma_{xy}&=2GH_s[-B_5(x,y,a)\\&\quad+yB_7(x,y,a)]+2GH_n[-yB_6(x,y,a)].\end{aligned}\tag{17}$$

It can be seen by comparing Eqs. (16) and (17) with Eqs. (2) and (3) that the displacements and stresses due to the crack-tip displacement discontinuity possess the same forms as those due to a constant displacement discontinuity, with $F_l(x,y,a)$ $(i=2,3,\ldots,7)$ in Eqs. (2) and (3) being replaced by $B_i(x,y,a)$ $(i=2,3,\ldots,7)$, and D_x and D_y by H_s and H_n, respectively. This enables the boundary element implementation to be easy.

The computation of B_i $(i=2,3,\ldots,7)$ in Eqs. (16) and (17) will be carried out in the following from four respects.

(1) For an arbitrary point $P(x,y)$ $(y\neq 0)$, generally, the analytical solutions of integrals (15) are obtained difficultly. In this paper, the Gauss numerical integration is used to calculate them. The following transformation is made:

$$\xi=at,\tag{18}$$

and then

$$\begin{aligned}B_i(x,y,a)&=\int_{-a}^{a}\left(\frac{a+\xi}{a}\right)^{1/2}V_i(x,y,\xi)d\xi\\&=a\int_{-1}^{1}V_i(x,y,at)(1+t)^{1/2}dt\quad(i=2,3,\ldots,7).\end{aligned}\tag{19}$$

Therefore, $B_i(x,y,a)$ can be given by

$$B_i(x,y,a)=a\sum_j V_i(x,y,a\zeta_j)(1+\zeta_j)^{1/2}w_j\quad(i=2,3,\ldots,7),\tag{20}$$

where ζ_i and w_i are the Gauss point coordinates and corresponding weighed factors, respectively.

(2) For an arbitrary point $P(x,y)$ $(y=0)$, integrals B_2, B_4, B_5, B_6, and B_7 in Eq. (14) can be solved analytically. For $x>-a$,

$$\begin{aligned}B_2(x,0,a)&=\frac{-1}{4\pi(1-\nu)}\left\{-2\sqrt{2}+\sqrt{\frac{x+a}{a}}\ln\left|\frac{\sqrt{x+a}+\sqrt{2a}}{\sqrt{x+a}-\sqrt{2a}}\right|\right\},\\B_4(x,0,a)&=0,\\B_5(x,0,a)&=\frac{1}{4\pi(1-\nu)}\left\{\frac{\sqrt{2}}{x-a}-\frac{1}{2\sqrt{a(x+a)}}\ln\left|\frac{\sqrt{x+a}+\sqrt{2a}}{\sqrt{x+a}-\sqrt{2a}}\right|\right\},\\B_6(x,0,a)&=\frac{1}{4\pi(1-\nu)}\left\{\frac{\sqrt{2}}{(x-a)^2}-\frac{\sqrt{2}}{2(x^2-a^2)}\right.\\&\quad\left.-\frac{1}{4\sqrt{a}(x+a)^{3/2}}\ln\left|\frac{\sqrt{x+a}+\sqrt{2a}}{\sqrt{x+a}-\sqrt{2a}}\right|\right\},\\B_7(x,0,a)&=0.\end{aligned}\tag{21}$$

While for $x<-a$, let r denote the distance from the crack tip along the crack extension line, i.e.,

$$r=|x|-a.\tag{22}$$

Then

$$B_2(x,0,a)=\frac{-1}{4\pi(1-\nu)}\left\{-2\sqrt{2}+2\sqrt{\frac{r}{a}}\arctan\sqrt{\frac{2a}{r}}\right\},$$

$$B_4(x,0,a)=0,$$

$$B_5(x,0,a)=\frac{1}{4\pi(1-\nu)}\left\{-\frac{\sqrt{2}}{r+2a}+\frac{1}{\sqrt{ar}}\arctan\sqrt{\frac{2a}{r}}\right\},\tag{23}$$

$$B_6(x,0,a)=\frac{1}{4\pi(1-\nu)}\left\{\frac{\sqrt{2}}{(r+2a)^2}-\frac{\sqrt{2}}{2r(r+2a)}-\frac{1}{2\sqrt{a}r^{3/2}}\arctan\sqrt{\frac{2a}{r}}\right\},$$

$$B_7(x,0,a)=0.$$

(3) For an arbitrary point $P(x,y)$ $(y=0)$, the integral B_3 in Eq. (14) is

$$B_3(x,0,a)=\begin{cases}0, & |x|>a\\ +\dfrac{1}{4(1-\nu)}, & y=0_+,\quad |x|<a\\ -\dfrac{1}{4(1-\nu)}, & y=0_-,\quad |x|<a\end{cases}\tag{24}$$

(4) From Eqs. (21) and (24), one can obtain the element self-effects easily:

$$B_2(0,0,a)=\frac{-1}{4\pi(1-\nu)}\left[-2\sqrt{2}+\ln\left|\frac{1+\sqrt{2}}{1-\sqrt{2}}\right|\right],$$

$$B_3(0,0,a)=\begin{cases}+\dfrac{1}{4(1-\nu)}, & y=0_+\\ -\dfrac{1}{4(1-\nu)}, & y=0_-\end{cases}$$

$$B_4(0,0,a)=0,\tag{25}$$

$$B_5(0,0,a)=\frac{1}{4\pi(1-\nu)}\left[-\sqrt{2}-\frac{1}{2}\ln\left|\frac{1+\sqrt{2}}{1-\sqrt{2}}\right|\right]\Big/\,a,$$

$$B_6(0,0,a)=\frac{1}{4\pi(1-\nu)}\left[-\frac{3\sqrt{2}}{2}-\frac{1}{4}\ln\left|\frac{1+\sqrt{2}}{1-\sqrt{2}}\right|\right]\Big/\,a^2,$$

$$B_7(0,0,a)=0.$$

For the right crack-tip displacement discontinuity element, similar formulas can be obtained and do not be given here.

2.4 Implementation of the Present Numerical Approach and Some Illustrations. Crouch and Starfied [20] used Eqs. (2) and (3) to set up the constant displacement discontinuity boundary element method (BEM). Similarly, we can use Eqs. (16) and (17) to set up boundary element equations associated with the crack-tip elements. The constant displacement discontinuity elements presented by Crouch and Starfield [20] together with the crack-tip elements presented in this paper are easily combined to form a very effective numerical approach for calculating the SIFs of general plane cracks. In the boundary element implementation, the left or the right crack-tip element is placed locally at the corresponding left or right crack tip on top of the constant displacement discontinuity elements that cover the entire crack surface and the other boundaries. The method is called as the HDDM.

The hybrid displacement discontinuity method presented in this paper differs from hybrid boundary element codes [27] that, when used to analyze the SIFs of a branched crack, require the plate to be modeled as a finite plate of huge dimensions by fictitious stress elements [20], while the crack could be modeled by displacement discontinuity elements. This brings about a higher computational effort.

Pan [28] pointed out that ''the displacement discontinuity method [20] is quite suitable for cracks in infinite domain where there is no no-crack boundary. However, it alone may not be efficient for finite domain problems, since the kernel functions in DDM involve singularities with order higher than those in the traditional displacement BEM.'' The hybrid displacement discontinuity method is used by the author to calculate the SIFs of complex plane cracks in a finite plate (e.g., a center slant cracked rectangular plate subjected to tension load; cracks emanating from an elliptical hole in a rectangular plate under biaxial loads). These numerical results show that the present numerical approach is also simple, yet very accurate. Because of the limitation to the length of this paper, these results are not reported here.

By the way, it is pointed out here that the displacement discontinuity boundary element program listed in Ref. [20] has one restriction concerning the placement of boundary elements in a problem involving symmetry: a boundary element cannot *lie along* a line of symmetry. Obviously, this restriction means that the symmetric conditions about the *x*-axis and *y*-axis for the crack problems shown in Figs. 7–9 cannot be used and that the symmetric condition about the *x*-axis for the crack problem shown in Fig. 5 cannot be used also. This leads to the result that when the program is used to analyze the crack problems shown in Figs. 5, 7, 8, and 9, it is not much more efficient than the hybrid displacement discontinuity method, which has no such restriction.

Table 1 Variation of SIFs for a center crack in an infinite plate with the number of elements

Number of elements	3	5	7	10	15	25
$K_1/\sigma\sqrt{\pi a}$	0.9621	0.9775	0.9838	0.9885	0.9921	0.995

3 Computational Formulas of Stress Intensity Factors and Simple Test Examples

The objective of many analyses of linear elastic crack problems is to obtain the SIFs K_{I} and K_{II}. Based on the displacement fields around the crack tip, the following formulas exist:

$$K_{\mathrm{I}}=-\frac{G\sqrt{2\pi}}{4(1-\nu)}\lim_{r\to 0}\{D_y(r)/r^{0.5}\},$$

$$K_{\mathrm{II}}=-\frac{G\sqrt{2\pi}}{4(1-\nu)}\lim_{r\to 0}\{D_x(r)/r^{0.5}\},\tag{26}$$

where $D_y(r)$ and $D_x(r)$ are the normal and shear components of displacement discontinuity at a distance r from the crack tip(s). For practical purposes, the limits in Eq. (26) can be approximated by simply evaluating the expression for a fixed value of r that is small in relation to the size of the crack. By means of the crack-tip displacement discontinuity functions defined in Eqs. (13), thus, the approximate formulas of the SIFs K_{I} and K_{II} can be obtained by letting r in Eqs. (26) be a, one-half length of the crack-tip element:

$$K_{\mathrm{I}}=-\frac{\sqrt{2\pi}GH_n}{4(1-\nu)\sqrt{a}},\quad K_{\mathrm{II}}=-\frac{\sqrt{2\pi}GH_s}{4(1-\nu)\sqrt{a}}.\tag{27}$$

To prove the efficiency of the suggested approach, two simple test examples are given here. An infinite plate with a through crack of length $2a$ that is subjected to uniform stress normal to the crack plane at distances sufficiently far away from the crack, is taken to compute the stress intensity factor K_{I}. Owing to its symmetry, only half is taken for the analysis. Table 1 gives the ratio of the numerical solution to the analytical stress intensity factor K_{I} as

Table 2 Variation of SIFs for a center crack in an infinite plate with the ratio of the size of the crack-tip element to that of constant elements

$a_{\text{crack}}/a_{\text{constant}}$	0.60	0.65	0.70	0.75	0.80	0.85	0.90	0.95	1.00
$K_1/\sigma\sqrt{\pi a}$	1.2048	1.1690	1.1394	1.1143	1.0928	1.0742	1.0578	1.0433	1.0303
$a_{\text{crack}}/a_{\text{constant}}$	1.05	1.10	1.15	1.20	1.25	1.30	1.35	1.40	1.45
$K_1/\sigma\sqrt{\pi a}$	1.0186	1.0080	0.9984	0.9896	0.9815	0.9741	0.9671	0.9607	0.9547

the number of elements is increased. In this calculation, the crack-tip element and constant elements are taken to be equal in size. Table 2 gives the ratio of the numerical solution to the analytical stress intensity factor K_I as the ratio of the size of the crack-tip element to the one of constant elements is changed. Here, the sizes of the constant elements are taken to be equal and the total number of elements is 11. It can be seen from Table 1 that a good result for the stress intensity factor K_I can be obtained using the crack-tip element. It can be seen from Table 2 that the ratio of the size of the crack-tip element to that of constant elements must be taken to be from 1.0 to 1.3 to obtain a good result with a relative error of less than 3%. This can be regarded as the limitation to the approach presented in the present article.

An inclined crack plate with a through crack of length $2a$ that is subjected to uniform stress at distances sufficiently far away from the crack is taken as another example to compute the SIFs K_I and K_{II}, whose exact solution is available [29]. Here, the SIFs K_I and K_{II} calculated by the present study are normalized by

$$K_I = F_I/(\sigma\sqrt{\pi a}\sin^2\beta), \quad K_{II} = F_{II}/(\sigma\sqrt{\pi a}\sin\beta\cos\beta), \tag{28}$$

where β is the angle between the load and the crack plane. Some numerical results are given in Table 3. In this calculation, the crack-tip elements and constant elements are taken to be the same size and the total number of elements is taken to be 20, i.e., two crack-tip elements and 18 constant elements. It is observed from Table 3 that regardless of the size of the angle β between the load and the crack plane, the present numerical results of the SIFs K_I and K_{II} are in good agreement with the analytical results.

4 Numerical Examples

From the 1970s to today, many researchers have paid attention to branched cracks [1–12], in particular, a singly branched crack. The investigation approaches for these include mostly the Muskhelishvili potential formulation [1,9,30], the conformal mapping method [6–8], the dislocation distribution method [12], and numerical methods, mostly, finite element methods [11,19] and boundary element methods [16,19,31,32]. Here, the present numerical approach is used to calculate the SIFs of branched cracks in an infinite sheet and the present numerical results are compared with the available solutions. Evidently, Bueckner's principle can be used in these analyses.

4.1 A Singly Branched Crack. First, the boundary-element method presented in this article is used to calculate the SIFs of a singly branched crack (see Fig. 1) in an infinite sheet under uniform tension. The SIFs at the branched crack tip B are normalized by

$$F_{IB} = K_{IB}/\sigma\sqrt{\pi c}, \quad F_{IIB} = K_{IIB}/\sigma\sqrt{\pi c} \tag{29}$$

Regarding the discretization of boundary elements, the number of elements discretized on the branched crack is varied with b/a (see Table 4), and the other boundaries are discretized according to the limitation condition that all boundary elements have approximately the same length. For the case of $b/a=0.01$, for example, 2000 elements, which have the same size $2a/2000$, are discretized on the main crack AO, and 10 elements, which have the same size $b/10$, are discretized on the branched crack OB. Here, $2a/2000=b/10$. The element number at the crack tip A is denoted by 1 and the element number at the crack tip B is denoted by 2010. Thus, the element 1 and the element 2010 are the left and the right crack-tip elements, respectively. The elements whose numbers are from 2 to 2009 are all common elements.

Table 5 shows the SIFs at the branched crack tip B obtained in the present article as the branched angle θ and b/a are changed. For comparative purposes, Table 6 lists the analytical results obtained by Kitagawa et al. [6,7] (also see p. 352 in Ref. [29]) by means of the conforming mapping method, whose conjecture has been proven by Lo [9] through the Muskhelishvili potential formulation. It can be seen from Tables 5 and 6 that the present numerical results are in extremely good agreement with those by Kitagawa et al. [6,7].

For a small singly branched crack ($b/a=0.01$), it can be seen by comparing the SIFs given from the present study with those by Kitagawa et al. [6,7] (also see p. 353 in the Ref. [29]) that the agreement is, respectively, within 0.7% and 4% for the stress intensity factors F_{IB} and F_{IIB} (see Table 7).

4.2 A Symmetrically Branched Crack. Second, the present numerical method is used to calculate the SIFs of a symmetrically branched crack (see Fig. 5) in an infinite sheet under uniform tension. The SIFs at the main crack tip A and at the branched crack tip B are normalized by

$$F_I^A = K_{IA}/\sigma\sqrt{\pi c}, \qquad F_I^B = K_{IB}/\sigma\sqrt{\pi c}, \quad F_{II}^B = K_{IIB}/\sigma\sqrt{\pi c}. \tag{30}$$

Regarding the discretization of boundary elements, the number of elements discretized on a branched crack is varied with b/a (see Table 8), and the other boundaries are discretized according to the limitation condition that all boundary elements have approximately the same length. Table 9 shows the present numerical results of the normalized SIFs at the main crack tip A and at the branched crack tip B as the branched angle θ and b/a are changed. For comparative purposes, Table 9 lists also the normalized SIFs given by Kitagawa et al. [6,7] (also see p. 374 in Ref. [29]) by means of the conforming mapping method, whose conjecture has been proven by Lo [9] through the Muskhelishvili potential formulation. It is found from Table 9 that the agreement is, respectively, within 1%, 2.4%, and 3% for the SIFs F_I^A, F_I^B, and F_{II}^B.

4.3 A Skew-Symmetric Branched Crack. Third, the SIFs of a skew-symmetric branched crack in an infinite sheet under

Table 3 Variation of SIFs for an inclined center crack in an infinite plate with the angle β

β	5 deg	10 deg	20 deg	30 deg	40 deg	45 deg	50 deg	60 deg	70 deg	80 deg	85 deg
F_I	0.9895	0.9898	0.9896	0.9898	0.9898	0.9885	0.9897	0.9897	0.9898	0.9897	0.9896
F_{II}	0.9896	0.9897	0.9897	0.9897	0.9897	0.9885	0.9897	0.9897	0.9897	0.9897	0.9896

Table 4 Variation of the number of elements discretized on a branched crack for a singly branched crack with b/a

b/a										
0.01	0.05	0.1	0.2	0.4	0.5	0.6	0.8	1.0	1.5	2.0
10	10	15	30	30	30	30	30	30	45	60

uniform tension (see Fig. 6) are analyzed by means of the present numerical approach. The SIFs at a branched crack tip are normalized by

$$F_{\mathrm{I}}=K_{\mathrm{I}}/\sigma\sqrt{\pi c},\quad F_{\mathrm{II}}=K_{\mathrm{II}}/\sigma\sqrt{\pi c}. \tag{31}$$

Regarding the discretization of boundary elements, the number of elements discretized on a branched crack is varied with b/a (see also Table 8), and the other boundaries are discretized according to the limitation condition that all boundary elements have approximately the same length. Table 10 shows the SIFs at the branched crack tip given by the present study and by Kitagawa et al. [6,7] (also see p. 362 in Ref. [29]) as the branched angle θ and b/a are changed. Evidently, the present numerical results are in extremely good agreement with those obtained by Kitagawa et al. [6,7] by using the conforming mapping method.

4.4 A Doubly Symmetrically Branched Crack. Finally, the SIFs of a doubly symmetrically branched crack in an infinite sheet under uniform tension (see Fig. 7) are analyzed by means of the present numerical approach. The SIFs at a branched crack tip are determined still by using formulas (31). Regarding the discretization of boundary elements, the number of elements discretized on a branched crack is varied with b/a (see also Table 8), and the other boundaries are discretized according to the limitation condition that all boundary elements have approximately the same length. Table 11 shows the SIFs at a branched crack tip as the branched angle θ and b/a are changed. For the comparison purpose, Table 11 lists also the SIFs at the branched crack tip obtained by Vitek [12] (also see p. 386 in Ref. [29] by means of the dislocation distribution method. It can be seen from Table 11 that for the doubly symmetric branched crack the present numerical results are in good agreement with those by Vitek within 2.2%.

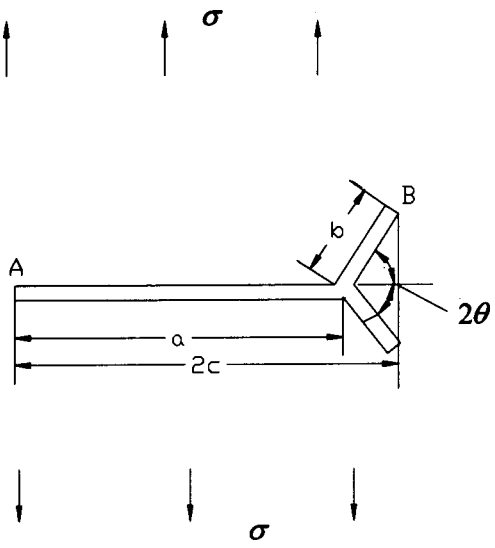

Fig. 5 A symmetrically branched crack

Table 5 Normalized SIFs at the branched crack tip B for a singly branched crack in the present study

	15 deg		30 deg		45 deg		60 deg	
b/a	$F_{\mathrm{I}B}$	$F_{\mathrm{II}B}$	$F_{\mathrm{I}B}$	$F_{\mathrm{II}B}$	$F_{\mathrm{I}B}$	$F_{\mathrm{II}B}$	$F_{\mathrm{I}B}$	$F_{\mathrm{II}B}$
0.01	0.9654	0.1614	0.8709	0.2995	0.7309	0.3964	0.5665	0.4422
0.05	0.9578	0.1938	0.8410	0.3572	0.6693	0.4667	0.4710	0.5105
0.1	0.9530	0.2131	0.8234	0.3918	0.6332	0.5096	0.4140	0.5527
0.2	0.9487	0.2349	0.8065	0.4314	0.5978	0.5595	0.3573	0.6037
0.4	0.9448	0.2554	0.7938	0.4689	0.5725	0.6076	0.3185	0.6539
0.5	0.9439	0.2607	0.7915	0.4786	0.5682	0.6197	0.3127	0.6655
0.6	0.9433	0.2644	0.7902	0.4852	0.5661	0.6277	0.3107	0.6724
0.8	0.9427	0.2688	0.7894	0.4929	0.5655	0.6363	0.3120	0.6775
1.0	0.9425	0.2710	0.7896	0.4966	0.5667	0.6395	0.3158	0.6766
1.5	0.9438	0.2729	0.7926	0.4992	0.5717	0.6388	0.3260	0.6668
2.0	0.9448	0.2726	0.7950	0.4981	0.5761	0.6351	0.3330	0.6563

Table 6 Normalized SIFs at the crack tip B for a singly branched crack by Kitagawa et al. [6,7]

	15 deg		30 deg		45 deg		60 deg	
b/a	$F_{\mathrm{I}B}$	$F_{\mathrm{II}B}$	$F_{\mathrm{I}B}$	$F_{\mathrm{II}B}$	$F_{\mathrm{I}B}$	$F_{\mathrm{II}B}$	$F_{\mathrm{I}B}$	$F_{\mathrm{II}B}$
0.1	0.9540	0.2120	0.8245	0.3895	0.6339	0.5053	0.4106	0.5462
0.2	0.9496	0.2346	0.8076	0.4307	0.5983	0.5578	0.3583	0.5996
0.4	0.9466	0.2556	0.7957	0.4690	0.5741	0.6072	0.3189	0.6514
0.6	0.9457	0.2648	0.7927	0.4858	0.5679	0.6283	0.3112	0.6718
0.8	0.9456	0.2694	0.7922	0.4940	0.5678	0.6375	0.3128	0.6770
1.0	0.9457	0.2718	0.7928	0.4981	0.5694	0.6413	0.3171	0.6775
1.5	0.9463	0.2737	0.7951	0.5008	0.5744	0.6414	0.3273	0.6682
2.0	0.9468	0.2733	0.7971	0.4996	0.5785	0.6377	0.3340	0.6580

Table 7 Normalized SIFs at the small branch crack tip B for a singly branched crack ($b/a=0.01$)

	$F_{\mathrm{I}B}$		$F_{\mathrm{II}B}$	
θ (deg)	Refs. [6], [7]	Present	Refs. [6], [7]	Present
15	0.971	0.9654	0.156	0.1614
30	0.876	0.8709	0.296	0.2995
45	0.732	0.7309	0.389	0.3964
60	0.569	0.5665	0.431	0.4422
75	0.404	0.4000	0.420	0.4368

5 Cracks Emanating From a Rhombus Hole in an Infinite Plate Under Biaxial Loads

In this section, specifically, the boundary element method presented in this article is used to study cracks emanating from a rhombus hole in an infinite plate under biaxial loads. The present numerical results for this crack problem indicate further that the present approach is very effective for calculating the SIFs of complex plane cracks and can reveal the effect of the biaxial load on the SIFs.

Shown in Fig. 8 is the schematic of cracks emanating from a rhombus hole in an infinite plate under biaxial loads. For this problem, symmetric conditions about the x-axis and y-axis can be used. The following cases are considered:

$$\lambda=0,1,-1$$

$$\theta=15\ \text{deg},\ 30\ \text{deg},\ 45\ \text{deg},$$

$$a/b=1.05,\ 1.1,\ 1.2,\ 1.4,\ 1.6,\ 1.8,\ 2.0,\ 2.5,\ 3.0,\ 4.0.$$

Regarding the discretization of boundary elements, the number of elements discretized on a quarter of rhombus hole is 100, and the other boundaries are discretized according to the limitation condition that all boundary elements have approximately the same

Table 8 Variation of the number of elements discretized on a branched crack for a symmetrically branched crack with b/a

b/a										
0.01	0.05	0.1	0.2	0.4	0.5	0.6	0.8	1.0	1.5	2.0
10	10	15	30	30	30	30	30	30	45	60

Table 9 Normalized SIFs for a symmetrically branched crack

		60 deg		45 deg		30 deg	
b/a		Refs. [6], [7]	Present	Refs. [6], [7]	Present	Refs. [6], [7]	Present
0.01	F_{I}^{A}		1.0001		0.9998		0.9994
	F_{I}^{B}		0.5390		0.6499		0.7138
	F_{II}^{B}		0.3158		0.2223		0.0913
0.05	F_{I}^{A}	1.01	1.0054	1.01	1.0043	1.01	1.0027
	F_{I}^{B}	0.45	0.4450	0.59	0.5918	0.70	0.6888
	F_{II}^{B}	0.39	0.3889	0.29	0.2994	0.15	0.1575
0.1	F_{I}^{A}	1.01	1.0097	1.01	1.0080	1.01	1.0057
	F_{I}^{B}	0.39	0.3899	0.56	0.5588	0.68	0.6764
	F_{II}^{B}	0.43	0.4362	0.34	0.3479	0.19	0.1985
0.2	F_{I}^{A}	1.02	1.0159	1.02	1.0135	1.01	1.0105
	F_{I}^{B}	0.34	0.3349	0.54	0.5268	0.66	0.6651
	F_{II}^{B}	0.49	0.4923	0.40	0.4042	0.24	0.2464
0.4	F_{I}^{A}	1.03	1.0248	1.02	1.0199	1.02	1.0155
	F_{I}^{B}	0.29	0.2944	0.51	0.5029	0.65	0.6564
	F_{II}^{B}	0.55	0.5451	0.46	0.4583	0.28	0.2938
0.5	F_{I}^{A}		1.0298		1.0227		1.0175
	F_{I}^{B}		0.2869		0.4982		0.6551
	F_{II}^{B}		0.5579		0.4728		0.3074
0.6	F_{I}^{A}	1.04	1.0355	1.03	1.0257	1.02	1.0192
	F_{I}^{B}	0.28	0.2829	0.50	0.4956	0.65	0.6545
	F_{II}^{B}	0.57	0.5658	0.49	0.4830	0.32	0.3175
0.8	F_{I}^{A}	1.05	1.0487	1.04	1.0320	1.03	1.0225
	F_{I}^{B}	0.28	0.2801	0.50	0.4933	0.65	0.6544
	F_{II}^{B}	0.58	0.5731	0.50	0.4957	0.33	0.3313
1.0	F_{I}^{A}	1.07	1.0632	1.04	1.0387	1.03	1.0255
	F_{I}^{B}	0.28	0.2802	0.50	0.4927	0.66	0.6548
	F_{II}^{B}	0.58	0.5742	0.51	0.5028	0.34	0.3402

length. The present numerical results of the SIFs normalized by $\sigma\sqrt{\pi a}$ are given in Table 12. For purposes of comparison, Table 12 also lists the numerical results in Ref. [29]. From Table 12, it is found that the present numerical results are in excellent agreement with those reported in Ref. [29]. From Table 12, it is found that the effect of the load parameter λ on the SIFs varies with θ and a/b and that the effect of the rhombus angle θ on the SIFs varies with load parameter λ and a/b.

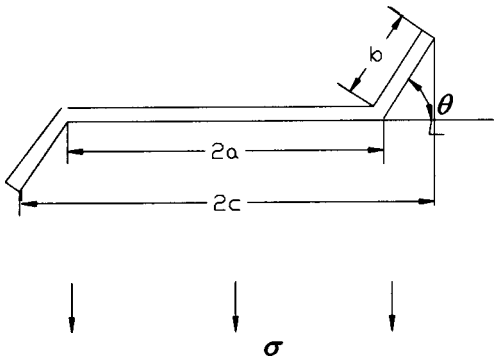

Fig. 6 A skew-symmetric branched crack

6 Numerical Simulation of Fatigue Crack Propagation Process Under Mixed-Mode Conditions

On the application of boundary element methods to crack propagation analysis, the first attempt to automatically model crack propagation under mixed-mode conditions was given by Ingraffea, Blanford, and Liggett [22] for two-dimensional problems. They used the multiregion method [13] together with the maximum circumferential stress criterion to calculate the direction of crack propagation. Aliabadi [23] pointed out that the difficulty with the multiregion method is that the introduction of artificial boundaries to divide the regions is not unique, and thus it is not easy to implement it in an automatic procedure. In an incremental crack extension analysis, these artificial boundaries must be repeatedly introduced for each increment of crack extension. Finite element simulations [25,26] when used to analyze crack problems

Table 10 Normalized SIFs at a branched crack tip for a skew-symmetric branched crack

	60 deg				45 deg				30 deg			
	Refs. [6], [7]		Present		Refs. [6], [7]		Present		Refs. [6], [7]		Present	
b/a	F_{I}	F_{II}	F_{I}	F_{II}	F_{I}	F_{II}	F_{I}	F_{II}	F_{I}	F_{II}	F_{I}	F_{II}
0.01	0.5905	0.4120	0.5936	0.4243	0.7485	0.3686	0.7485	0.3772	0.8809	0.2780	0.8792	0.2834
0.05	0.5232	0.4610	0.5274	0.4731	0.7058	0.4184	0.7069	0.4268	0.8603	0.3182	0.8600	0.3236
0.1	0.4822	0.4920	0.4853	0.5022	0.6805	0.4507	0.6811	0.4560	0.8483	0.3436	0.8479	0.3469
0.2	0.4306	0.5350	0.4384	0.5391	0.6532	0.4888	0.6532	0.4913	0.8356	0.3727	0.8351	0.3741
0.4	0.3934	0.5794	0.3944	0.5830	0.6280	0.5284	0.6273	0.5303	0.8242	0.4021	0.8231	0.4032
0.6	0.3734	0.6031	0.3737	0.6062	0.6161	0.5491	0.6150	0.5508	0.8187	0.4176	0.8172	0.4184
0.8	0.3629	0.6170	0.3626	0.6197	0.6095	0.5617	0.6080	0.5630	0.8156	0.4271	0.8137	0.4277
1.0	0.3570	0.6253	0.3564	0.6278	0.6054	0.5698	0.6036	0.5709	0.8135	0.4335	0.8114	0.4340

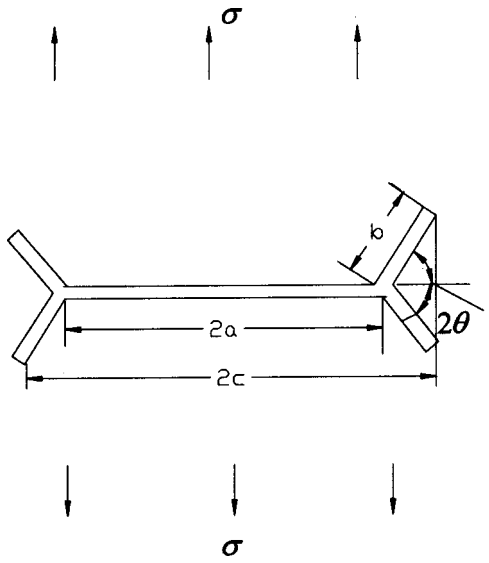

Fig. 7 A doubly symmetrically branched crack

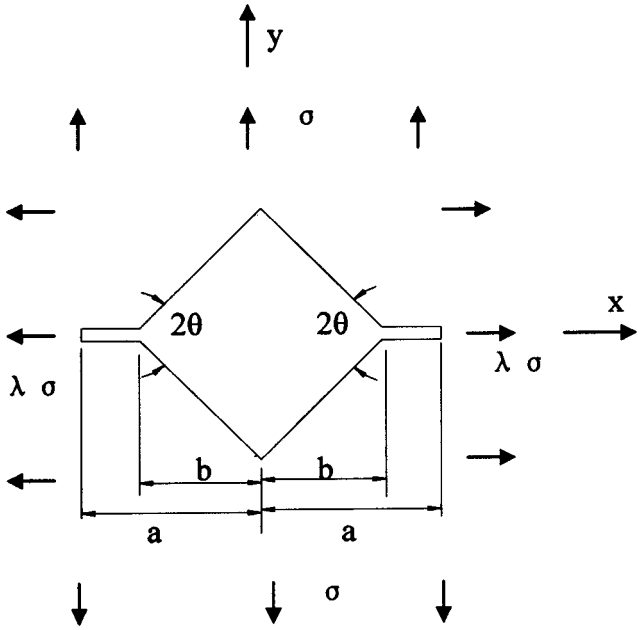

Fig. 8 Cracks emanating from a rhombus hole in an infinite plate under biaxial loads

have to face difficult computational problems connected with the discretization of the continuum into finite elements, particularly when some cracks propagate, thus changing the interior boundaries of the solids.

In this paper, the hybrid displacement discontinuity method and the maximum circumferential stress criterion [24] are combined to form a very effective numerical approach for simulating the fatigue crack propagation process in plane elastic bodies under mixed-mode conditions. In the numerical simulation, for each increment of crack extension, remeshing of existing boundaries is not required because of an intrinsic feature of the HDDM. Crack propagation is simulated by adding new boundary elements on the incremental crack extension to the previous crack boundaries. At the same time, the element characters of some related elements are adjusted according to the manner in which the boundary element method is implemented. As an example, the fatigue propagation process of cracks emanating from a circular hole in a plane elastic plate is simulated using the numerical simulation approach.

It is well known that the fatigue crack propagation, which propagates in a self-similar manner, obeys Paris's equation

$$\Delta a/\Delta N = A(\Delta K_{\mathrm{I}})^m, \tag{32}$$

where $\Delta a/\Delta N$ is the fatigue crack propagation ratio, A and m are material constants, and ΔK_{I} is the range of the stress intensity factor K_{I}.

In general, the fatigue propagation analysis of a crack under mixed-mode conditions involves the determination of the crack propagation direction (e.g., Sih and Barthelemy [33]) except for an equation similar to Eq. (32). Here, the fatigue propagation of a crack under mixed-mode conditions is assumed to satisfy the following conditions:

(1) A fatigue crack will propagate to the direction of the maximum tangential stress surrounding the crack tip.
(2) The fatigue crack propagation rate equation is

$$\frac{\Delta a}{\Delta N} = C(\Delta K_e)^n, \tag{33}$$

where

$$\Delta K_e = \tfrac{1}{2}\cos\frac{\theta_0}{2}[\Delta K_{\mathrm{I}}(1+\cos\theta_0) - 3\Delta K_{\mathrm{II}}\sin\theta_0], \tag{34}$$

where θ_0 is the crack propagation angle predicted according to condition (1), ΔK_{I} and ΔK_{II} are, respectively, the ranges of the stress intensity factors K_{I} and K_{II}, and C and n are material constants that are related to the material constants A and m in Paris's equation (32) by the relations

$$C = A, \quad n = m. \tag{35}$$

As an example, the fatigue propagation process of cracks emanating from a circular hole (see Fig. 9) in an infinite plate sub-

Table 11 Normalized SIFs for a doubly symmetric branched crack

	60 deg				45 deg				30 deg			
	F_{I}		F_{II}		F_{I}		F_{II}		F_{I}		F_{II}	
b/a	Vitek	Present	Vitek	Present	Vitek	Present	Vitek	Present	Vitek	Present	Vitek	Present
0.01	0.557	0.5664	0.292	0.2980	0.662	0.6685	0.200	0.2029	0.724	0.7240	0.073	0.0742
0.05	0.491	0.5014	0.350	0.3565	0.627	0.6348	0.262	0.2646	0.718	0.7188	0.125	0.1258
0.1	0.452	0.4615	0.394	0.3984	0.611	0.6184	0.307	0.3081	0.723	0.7240	0.162	0.1611
0.2	0.410	0.4184	0.454	0.4576	0.600	0.6074	0.368	0.3686	0.740	0.7419	0.211	0.2096
0.4		0.3830		0.5371		0.6127		0.4502		0.7839		0.2745
0.5	0.370	0.3764	0.562	0.5665	0.616	0.6208	0.481	0.4813	0.807	0.8060	0.301	0.2993
0.6		0.3736		0.5916		0.6307		0.5085		0.8282		0.3212
0.8		0.3749		0.6332		0.6532		0.5551		0.8719		0.3589
1.0	0.377	0.3810	0.663	0.6673	0.676	0.6774	0.591	0.5946	0.919	0.9144	0.393	0.3911

Table 12 Normalized SIFs for cracks emanating from a rhombus hole in an infinite plate under biaxial loads

	$\lambda=0$				$\lambda=-1$			$\lambda=+1$		
a/b	$\theta=15$ deg	$\theta=30$ deg	$\theta=45$ deg	$\theta=45$ deg [29]	$\theta=15$ deg	$\theta=30$ deg	$\theta=45$ deg	$\theta=15$ deg	$\theta=30$ deg	$\theta=45$ deg
1.05	1.0146	1.0389	1.0433		1.0313	1.1208	1.2461	0.9979	0.9570	0.8405
1.1	1.0105	1.0372	1.0602	1.07	1.0237	1.1072	1.2487	0.9973	0.9672	0.8717
1.2	1.0066	1.0305	1.0639	1.069	1.0157	1.0834	1.2229	0.9975	0.9776	0.9049
1.4	1.0031	1.0202	1.0535	1.058	1.0081	1.0530	1.1667	0.9981	0.9874	0.9403
1.6	1.0015	1.0137	1.0423	1.046	1.0046	1.0354	1.1244	0.9984	0.9920	0.9602
1.8	1.0005	1.0095	1.0333	1.037	1.0025	1.0244	1.0941	0.9985	0.9946	0.9725
2.0	1.0000	1.0067	1.0264	1.030	1.0013	1.0173	1.0723	0.9987	0.9961	0.9805
2.5	0.9993	1.0028	1.0150		0.9998	1.0078	1.0393	0.9988	0.9978	0.9907
3.0	0.9989	1.0009	1.0087		0.9991	1.0034	1.0225	0.9987	0.9984	0.9949
4.0	0.9986	0.9993	1.0027		0.9986	1.0000	1.0079	0.9986	0.9986	0.9975

jected to uniform cycle stress in the y direction at distances sufficiently far away from the hole is simulated. For this crack problem, the symmetric conditions about the x and y-axes can be used. In this analysis, the shear modulus G, Poisson's ratio ν, the fracture toughness K_{Ic}, the material constants A and m in Paris's equation, the threshold value of the stress intensity factor, ΔK_{th}, cyclic loading parameters, the mean stress σ_m, and the characteristic of cyclic loading, R, are as follows:

$$G=2744 \text{ kg/mm}^2, \quad \nu=0.321, \quad K_{Ic}=116 \text{ kg/mm}^{3/2},$$

$$A=1.039\times 10^{-10},$$

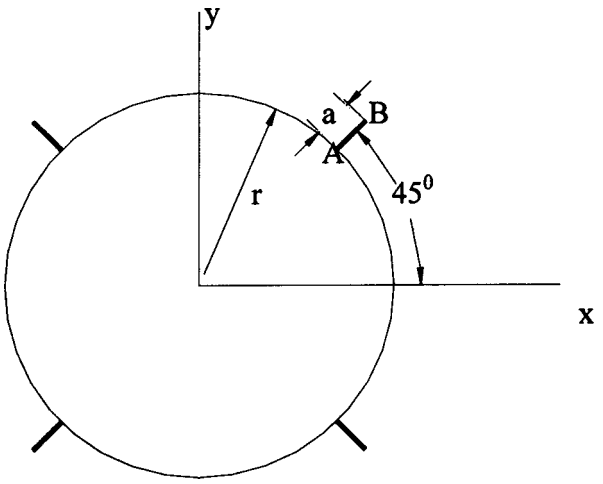

Fig. 9 Cracks emanating from a circular hole in an infinite plate

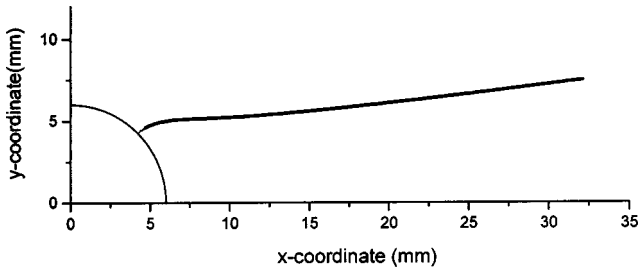

Fig. 10 Fatigue growth path of crack *AB* emanating from the circle hole for the case of $r=6$ mm

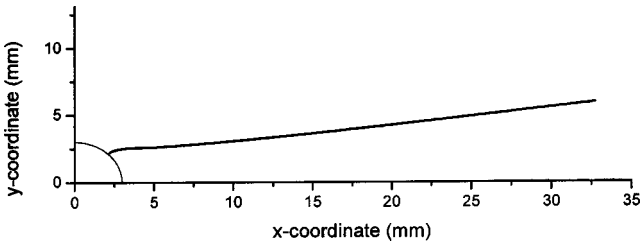

Fig. 11 Fatigue growth path of crack *AB* emanating from the circle hole for the case of $r=3$ mm

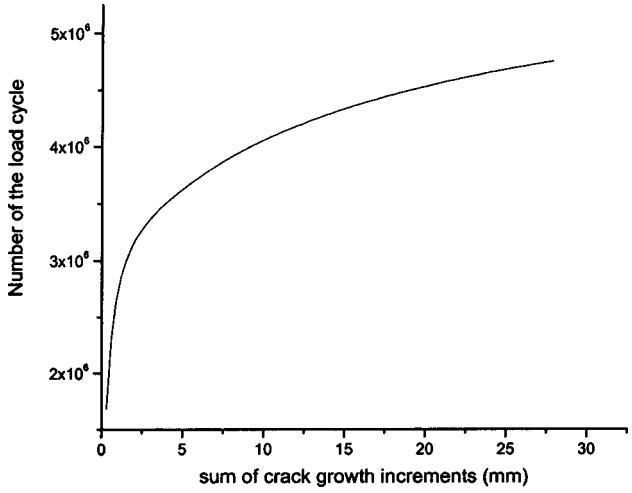

Fig. 12 Variation of the number of load cycle with crack growth for the case of $r=6$ mm

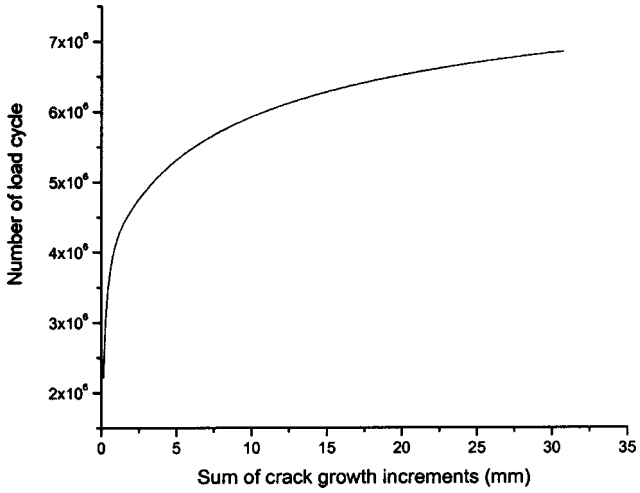

Fig. 13 Variation of the number of load cycle with crack growth for the case of $r=3$ mm

$$m=2.7438, \quad \Delta K_{\text{th}}=0, \quad \sigma_m=15.333 \ \text{kg/mm}^2, \quad R=0.048,$$

The geometric parameters considered here are

$$R=3 \ \text{mm}, \quad a/r=1/20.$$

$$r=6 \ \text{mm}, \quad a/r=1/20.$$

Some numerical results are given in Figs. 10–13. Shown in Figs. 10 and 11 are, respectively, the fatigue propagation path of crack *AB* emanating from the circle hole for the cases of $r=6$ and 3 mm. Shown in Figs. 12 and 13 are, respectively, the variation of the number of the load cycle with the crack propagation for the cases of $r=6$ and 3 mm.

7 Conclusions

In the present paper, the crack-tip displacement discontinuity elements are presented to model the singularity of stress near a crack tip. Furthermore, the crack-tip elements and the constant displacement discontinuity element presented by Crouch and Starfied are combined to form a numerical approach for calculating the SIFs of general plane cracks. Numerical examples are given and compared with the available solutions. It can be seen that the numerical approach is simple, yet very accurate for calculating the SIFs of branched cracks. As a new example, cracks emanating from a rhombus hole in an infinite plate under biaxial loads are taken into account. The numerical results indicate the efficiency of the present numerical approach and can reveal the effect of the biaxial load on the SIFs. In addition, the hybrid displacement discontinuity method developed in this paper together with the maximum circumferential stress criterion becomes a very effective numerical approach for simulating the fatigue crack propagation process in plane elastic bodies under mixed-mode conditions.

Acknowledgment

Special thanks are due to the National Natural Science Foundation of China (No. 10272037) and the Natural Science Foundation of Heilongjiang, China (No. A-02-05) for supporting the present work.

References

[1] Cotterel, B., and Rice, J. R., 1980, "Slightly Curved or Kinked Cracks," Int. J. Fract., **16**, pp. 155–169.
[2] Anderdon, H., and Erratum, W. G., 1969, "Stress Intensity Factors at the Tips of a Star-Shape Contour in an Infinite Tensile Sheet," J. Mech. Phys. Solids, **17**, pp. 405–417.
[3] Palaniswamy, K., and Knauss, W. G., "On the Problem of Crack Extension in Brittle Solids under General Loading," Report No. SM74-8, Graduate Aeronautical Lab., Caltech.
[4] Billy, B. A., and Cardew, G. E., 1975, "The Crack with a Kinked Tip," Int. J. Fract., **11**, pp. 708–711.
[5] Billy, B. A., Cardew, G. E., and Howard, I. C., 1977, "Stress Intensity Factors at the Tips of Kinked and Forked Cracks," in *Fracture 1977*, Taplin, D. M. R., ed., University of Waterloo Press, Canada, Vol. 3, pp. 197–200.
[6] Kitagawa, H., and Yuuki, R., 1977, "Analysis of Branched Cracks Under Biaxial Stresses," in *Fracture 1977*, Taplin D. M. R., eds., University of Waterloo Press, Canada, Vol. 3, pp. 201–211.
[7] Kitagawa, H., Yuuki, R., and Ohira, T. C., 1975, "Crack-Morphological Aspects in Fracture Mechanics," Eng. Fract. Mech., **7**, pp. 515–529.
[8] Chatterjee, S. N., 1975, "The Stress Field in the Neighborhood of a Branched Crack in an Infinite Sheet," Int. J. Solids Struct., **11**, pp. 521–538.
[9] Lo, K. K., 1978, "Analysis of Branched Cracks," ASME J. Appl. Mech., **45**, pp. 797–802.
[10] Theocaris, P. S., and Loakimidis, N., 1976, "The Symmetrically Branched Cracks in an Infinite Elastic Medium," ZAMP, **27**, pp. 801–814.
[11] Wilson, W. K., and Cherepko, J., 1983, "Analysis of Cracks With Multiple Branches," Int. J. Fract., **22**, pp. 302–315.
[12] Vitek, V., 1977, "Plane Strain Stress Intensity Factors for Branched Cracks," Int. J. Fract., **13-4**, pp. 481–510.
[13] Blandford, G. E., Ingraffea, A. R., and Liggett, J. A., 1981, "Two-Dimensional Stress Intensity Factor Computations Using the Boundary Element Method," Int. J. Numer. Methods Eng., **17**, pp. 387–404.
[14] Balas, J., Sladek, J., and Sladek, V., 1989, *Stress Analysis by Boundary Element Methods*, Elsevier, Amsterdam.
[15] Hong, H., and Chen, J., 1988, "Derivatives of Integral Equations of Elasticity," J. Eng. Mech., **114**, pp. 1028–1044.
[16] Portela, A., and Aliabadi, M. H., 1992, "The Dual Boundary Element Method: Effective Implementation for Crack Problems," Int. J. Numer. Methods Eng., **33**, pp. 1269–1287.
[17] Tanaka, M., and Itoh, H., 1987, "New Crack Elements for Boundary Element Analysis of Elastostatics Considering Arbitrary Stress Singularities," Appl. Math. Model., **11**, pp. 357–363.
[18] Cruse, T. A., 1989, *Boundary Element Analysis in Computational Fracture Mechanics*, Kluwer, Dordrecht.
[19] Aliabadi, M. H., and Rooke, D. P., 1991, *Numerical Fracture Mechanics*, Computational Mechanics Publications, Southampton and Kluwer, Dordrecht.
[20] Crouch, S. L., and Starfield, A. M., 1983, *Boundary Element Method in Solid Mechanics with Application in Rock Mechanics and Geological Mechanics*, Allen and Unwin, London.
[21] Crouch, S. L., 1976, "Solution of Plane Elasticity Problems by Displacement Discontinuity Method," Int. J. Numer. Methods Eng., **10**, pp. 301–343.
[22] Ingraffea, A. R., Blandford, G., and Liggett, J. A., 1987, "Automatic Modeling of Mixed-Mode Fatigue and Quasi-Static Crack Propagation Using the Boundary Element Method," 14th Natl. Symp. on Fracture, ASTM STP 791, pp. 1407–1426.
[23] Aliabadi, M. H., 1997, "Boundary Element Formulation in Fracture Mechanics," Appl. Mech. Rev., **50**, pp. 83–96.
[24] Erdogan, F., and Sih, G. C., 1963, "On the Crack Extension in Plates Under Plane Loading and Transverse Shear," J. Basic Eng., **85**, pp. 519–527.
[25] Charambides, P. G., and McMeeking, R. M., 1987, "Finite Element Method Simulation of a Crack Propagation in a Brittle Microcracked Solid," Mech. Mater., **6**, pp. 71–87.
[26] Huang, X., and Karihaloo, B. L., 1993, "Interaction of Penny Shaped Cracks With a Half Plane Crack," Int. J. Solids Struct., **25**, pp. 591–607.
[27] Scavia, C., 1992, "A Numerical Technique for the Analysis of Cracks Subjected to Normal Compressive Stresses," Int. J. Numer. Methods Eng., **33**, pp. 929–942.
[28] Pan, E., 1997, "A General Boundary Element Analysis of 2-D Linear Elastic Fracture Mechanics," Int. J. Fract., **88**, pp. 41–59.
[29] Murakami, Y., 1987, *Stress Intensity Factors Handbook*, Pergamon, New York.
[30] Chen, Y. Z., 1999, "Stress Intensity Factors for Curved and Kinked Cracks in Plane Extension," Theor. Appl. Fract. Mech., **31**, pp. 223–232.
[31] Liu, N., Altiero, N. J., and Sur, U., 1990, "An Alternative Integral Equation Approach Applied to Kinked Cracks in Finite Plane Bodies," Comput. Methods Appl. Mech. Eng., **84**, pp. 211–226.
[32] Denda, M., and Dong, Y. F., 1999, "Analytical Formulas for a 2-D Crack-Tip Singular Boundary Element for Rectilinear Cracks and Crack Growth Analysis," Eng. Anal. Boundary Elem., **23**, pp. 35–49.
[33] Sih, G. C., and Barthelemy, B. M., 1980, "Mixed Mode Fatigue Crack Growth Prediction," Eng. Fract. Mech., **13**, pp. 439–451.